Modeling Unconventional Superconductivity at the Crossover between Strong and Weak Electronic Interactions

Morten H. Christensen,[1,‡] Xiaoyu Wang,[2,‡] Yoni Schattner,[3,†] Erez Berg,[4] and Rafael M. Fernandes[1,*]
[1]School of Physics and Astronomy, University of Minnesota, Minneapolis, Minnesota 55455, USA
[2]National High Magnetic Field Laboratory, Tallahassee, Florida 32310, USA
[3]Department of Physics, Stanford University, Stanford, California 94305, USA
[4]Department of Condensed Matter Physics, Weizmann Institute of Science, Rehovot 76100, Israel

(Received 10 August 2020; accepted 22 October 2020; published 7 December 2020)

High-temperature superconductivity emerges in many different quantum materials, often in regions of the phase diagram where the electronic kinetic energy is comparable to the electron-electron repulsion. Describing such intermediate-coupling regimes has proven challenging as standard perturbative approaches are inapplicable. Here, we employ quantum Monte Carlo methods to solve a multiband Hubbard model that does not suffer from the sign problem and in which only repulsive interband interactions are present. In contrast to previous sign-problem-free studies, we treat magnetic, superconducting, and charge degrees of freedom on an equal footing. We find an antiferromagnetic dome accompanied by a metal-to-insulator crossover line in the intermediate-coupling regime, with a smaller superconducting dome appearing in the metallic region. Across the antiferromagnetic dome, the magnetic fluctuations change from overdamped in the metallic region to propagating in the insulating region. Our findings shed new light on the intertwining between superconductivity, magnetism, and charge correlations in quantum materials.

DOI: 10.1103/PhysRevLett.125.247001

Introduction.—While the problem of interacting electrons is well-understood in the regimes where the electron-electron repulsion is much smaller or much larger than the kinetic energy, the regime where both energy scales are comparable has remained elusive. It is precisely in this regime that several unique electronic collective phenomena are observed, high-temperature superconductivity being their poster child. In the cuprates, for example, the highest superconducting (SC) transition temperatures take place as the system moves from a Mott insulating to a Fermi liquid behavior [1]. In superconducting iron pnictides, although electronic interactions do not seem strong enough to localize the electrons, they can significantly reduce the coherence of the electronic quasiparticles [2–4]. Notwithstanding the appeal of constructing materials-specific models that can quantitatively describe and predict the properties of a moderately correlated compound, the challenges in describing this regime and its prevalence in several materials of interest warrant the investigation of minimal models that focus on key ingredients of the problem.

The Hubbard model is perhaps the most famous such minimal model, in which electrons hopping on a lattice are subject to an on-site repulsion that mimics a strongly screened Coulomb interaction. In the face of the difficulties in analyzing the intermediate-coupling regime analytically, numerical methods such as dynamical mean-field theory [5–8], density matrix renormalization group [9–11], or quantum Monte Carlo (QMC) [12–19] have been extensively applied. The main advantage of the latter is that it is an exact and unbiased method and that it is not limited to a one-dimensional geometry. However, it is intrinsically subject to the fermionic sign problem [20,21], which restricts the electronic occupation and temperature ranges that can be efficiently simulated. Another popular minimal model is the so-called spin-fermion model [22]. In this case, the electron-electron interaction is substituted in lieu of a collective bosonic antiferromagnetic (AFM) order parameter that can be fine-tuned to quantum criticality. This is motivated by the fact that AFM order is often observed in moderately coupled quantum materials in proximity to unconventional superconductivity. It was recently realized that versions of the spin-fermion model with two electronic flavors (such as two bands) possess a symmetry that eliminates the sign problem [23]. This has led to a flurry of QMC studies of spin-fermion and related boson-fermion models, which revealed a nearly universal enhancement of superconductivity at the bosonic quantum critical point [24–30]. However, in these models, the AFM order is introduced *ad hoc* rather than being treated on an equal footing with SC and other electronic orders.

In this Letter, we construct a model free of the fermionic sign problem in which we can treat all degrees of freedom on an equal footing. As a function of the strength of the electronic repulsion, we find an AFM dome intercepted by a metal-to-insulator crossover line at high temperatures.

As temperature is lowered, this crossover line eventually becomes a first-order phase transition as it merges with the magnetic dome. Crucially, a superconducting dome only emerges near one edge of the AFM dome, providing valuable information about the nature of the pairing mechanism. We attribute this to the overdamped nature of the spin fluctuations in this region. In contrast, in the region where no SC emerges, spin fluctuations propagate ballistically and cannot mediate sufficient pairing attractions.

Microscopic interacting model.—Motivated by the insight that led to the elimination of the sign problem from spin-fermion models [21,23], we consider a simple extension of the square-lattice Hubbard model to two bands. Starting from the two-orbital Hubbard–Kanamori Hamiltonian [4,31] and projecting onto states near the Fermi level, one generally obtains five distinct electron-electron interactions, U_i [32,33]. Physically, they correspond to intraband (U_4, U_5) and interband (U_1) repulsion, spin-exchange coupling (U_2), and pair-exchange coupling (U_3). Specifically, the Hamiltonian is given by $\mathcal{H} = \mathcal{H}_0 + \mathcal{H}_{\text{int}}$, with

$$\mathcal{H}_0 = \sum_{\mathbf{k}\alpha} \epsilon^c(\mathbf{k}) c^\dagger_{k\alpha} c_{\mathbf{k}\alpha} + \sum_{k\alpha} \epsilon^d(\mathbf{k}) d^\dagger_{\mathbf{k}\alpha} d_{\mathbf{k}\alpha} \tag{1}$$

$$\begin{aligned}\mathcal{H}_{\text{int}} = \sum_{i\alpha\beta} \Big[& U_1 c^\dagger_{i\alpha} c_{i\alpha} d^\dagger_{i\beta} d_{i\beta} + U_2 c^\dagger_{i\alpha} d^\dagger_{i\beta} c_{i\beta} d_{i\alpha} \\ & + \frac{U_3}{2} (c^\dagger_{i\alpha} c^\dagger_{i\beta} d_{i\beta} d_{i\alpha} + \text{H.c.}) \\ & + U_4 c^\dagger_{i\alpha} c^\dagger_{i\beta} c_{i\beta} c_{i\alpha} + U_5 d^\dagger_{i\alpha} d^\dagger_{i\beta} d_{i\beta} d_{i\alpha} \Big],\end{aligned} \tag{2}$$

where the operators c and d refer to the two bands, α and β are spin indices, and i and $\mathbf{k}$ are, respectively, real- and momentum-space indices. The square-lattice band dispersions $\epsilon^{c,d}(\mathbf{k}) = -2(t \pm \delta)\cos k_x a - 2(t \mp \delta)\cos k_y a \mp \mu$ are parameterized by the nearest-neighbor hopping coefficient t, a hopping anisotropy δ, and the chemical potential μ (see inset in Fig. 1). Here we set $\delta = 0.4t$, $\mu = -2t$, and the lattice parameter to $a = 1$. As we show in the Supplemental Material [34], this Hamiltonian is amenable to sign-problem-free QMC simulations if we consider only interband interactions, i.e., $U_4 = U_5 = 0$, impose the relations $U_1/4 = U_2/2 = U_3/2 = U > 0$, and constrain the spin indices in the U_1 term to $\beta = \alpha$. This latter constraint can be interpreted as a "single-ion" spin anisotropy, which, in addition to allowing sign-problem-free QMC simulations to be carried out, also allows for magnetic order to be stabilized at finite temperatures. Under these conditions, the Hamiltonian can be rewritten as

$$\mathcal{H} = \mathcal{H}_0 - U \sum_i S^z_i S^z_i, \tag{3}$$

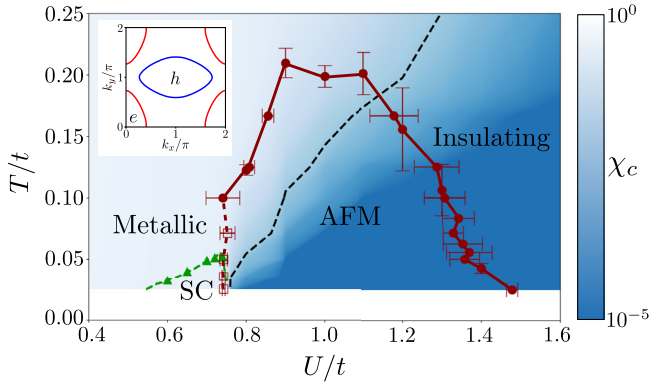

FIG. 1. Phase diagram obtained from thermodynamic observables. In the vicinity of $U/t \sim 1$, the phase diagram shows a variety of electronic phases, including AFM, SC, and a transition between metallic and insulating behaviors. No other ordered phases were observed for $0 \leq U \leq 4t$. The dark red full circles mark the magnetic transitions determined from a scaling analysis. Near $U/t \approx 0.75$ for $T/t < 0.1$, we find that the transition becomes first order (see Supplemental Material [34]), which is indicated by empty squares and a dashed red line. The color scale is logarithmic and corresponds to the compressibility χ_c [see Fig. 2(c)], while the black dashed line marks the contour $\chi_c = 0.01$. We interpret this near complete suppression of the compressibility as a sign of insulating behavior. The green triangles mark the superconducting critical temperatures obtained from the Berezinskii–Kosterlitz–Thouless criterion for the system size $L = 12$; the green dashed line is an interpolation. The inset shows the simulated band structure, exhibiting one electron pocket centered at (0,0) and one hole pocket centered at (π, π).

where

$$S^z_i = c^\dagger_{i\alpha} \sigma^z_{\alpha\beta} d_{i\beta} + \text{H.c.} \tag{4}$$

Note that the above constraints are much less severe than the particle-hole symmetry that has to be imposed on the single-band Hubbard model to avoid the sign problem. In contrast, here there are no restrictions on the electron filling of each band or on their dispersions. Importantly, as we show below, the interband interactions alone are sufficient to drive a plethora of ordered phases typically seen in quantum materials of interest, such as insulating behavior, magnetism, and superconductivity.

The inset in Fig. 1 depicts the specific band structure used in this work, consisting of elliptical electronlike and holelike bands at the center and at the corner of the Brillouin zone. This dispersion was chosen so that the Hamiltonian is invariant under fourfold rotations followed by particle-hole exchange and a (π, π) translation in momentum space. The choice of parameters implies $\langle n^c_i + n^d_i \rangle = 2$ but $n^c_i \neq n^d_i$, where $n^{c,d}_i$ is the electronic density of c (d) electrons at site i. The elliptical shape of the Fermi surfaces was selected to suppress nesting that would otherwise favor AFM. While we performed extensive QMC simulations only for this set of band parameters,

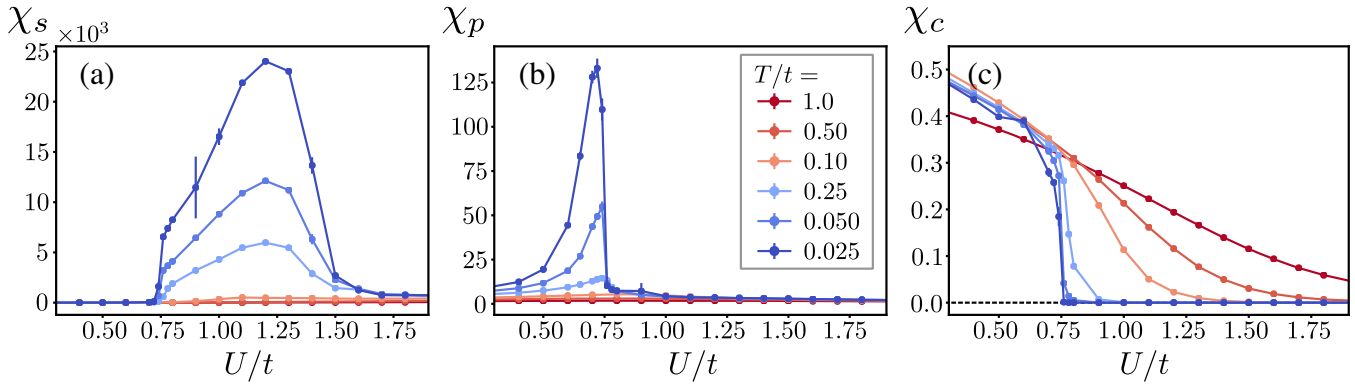

FIG. 2. Thermodynamic observables in the vicinity of $U/t \sim 1$. (a) AFM spin, (b) pair, and (c) charge susceptibilities (denoted by χ_s, χ_p, and χ_c, respectively) for different temperatures as a function of U/t. The pair susceptibility peaks in the immediate vicinity of the AFM transition. At low temperatures, within our resolution, we cannot separate the transition to the AFM phase from the crossover to the insulating phase.

simulations over narrower parameter ranges were also performed for modified band parameters, yielding similar phase diagrams.

Phase diagram.—The phase diagram of the microscopic model shown in Fig. 1 was obtained from determinant QMC simulations on $L \times L$ lattices with $L = 8, 10, 12, 14$ and for temperatures $T/t \geq 0.025$. Additional details of the simulation are presented in the Supplemental Material [34]. The salient feature of the phase diagram is an antiferromagnetic dome (red curve) in the intermediate coupling regime $U \sim t$. Indeed, as shown in Fig. 2(a), the AFM spin susceptibility at the wave vector $\mathbf{Q} = (\pi, \pi)$, $\chi_s = 4U^2 \langle \int d\tau S^z(\mathbf{Q}, \tau) S^z(-\mathbf{Q}, \tau = 0) \rangle + 2U$, displays a sharp enhancement at low temperatures above a critical interaction strength $U/t \approx 0.75$, followed by a smoother suppression near $U/t \approx 1.5$. The AFM phase boundary in Fig. 1 was determined using standard finite-size scaling analysis appropriate for an Ising-type transition considering the pairs of system sizes $L = (8, 12)$ and $L = (10, 14)$ [43]. For $T/t < 0.1$, we find evidence that the magnetic transition becomes first order near $U/t \approx 0.75$ (see Supplemental Material [34]). At higher temperatures and interaction strengths, the magnetic transition appears continuous. For $U/t > 1.5$, no AFM transition was observed down to the lowest temperature probed. We verified that even in the nonmagnetic state, the magnetic susceptibility remains peaked at the AFM wave vector $\mathbf{Q} = (\pi, \pi)$.

In addition to the AFM dome, we also found a much narrower SC dome in the vicinity of $U/t = 0.75$, i.e., near one of the putative AFM quantum phase transitions. The green triangles and green dashed line denote the SC transition temperatures T_c as determined by the Berezinskii–Kosterlitz–Thouless criterion, $\rho_s(T_c) = 2T_c/\pi$ for $L = 12$, interpolated between neighboring points. Importantly, this is an unconventional SC state with gaps of opposite signs in the two bands. Figure 2(b) shows the behavior of the corresponding pair susceptibility, $\chi_p = L^{-2} \sum_{ij} \int d\tau \langle P^\dagger_{\pm,i}(\tau) P_{\pm,j}(0) \rangle$, where $P_{\pm,i} = 2(c_{i\uparrow} c_{i\downarrow} - d_{i\uparrow} d_{i\downarrow})$ as a function of U and T. Its main features are the sharp peak observed slightly below $U/t = 0.75$, where the AFM dome begins, and the absence of any enhancement near $U/t = 1.5$, where the AFM dome ends. Within our resolution, the transition between the SC and AFM states appears first order. The sharp suppression in the pair susceptibility indicates that any coexistence of the two phases is limited to a narrow range of U/t in the vicinity of $U/t \approx 0.75$, although we observe no such coexistence within our resolution.

To shed light on the behavior of the charge degrees of freedom across the phase diagram, we extracted the charge compressibility, $\chi_c = L^{-2} \int d\tau \sum_{ij} \langle \delta\rho_i(\tau) \delta\rho_j(0) \rangle$, where $\delta\rho_i = n_i^c + n_i^d - 2$. As shown in Fig. 2(c), for $U/t \approx 0.75$, when AFM order sets in, χ_c displays a sudden drop at low temperatures from a finite value, indicative of a metal, to a vanishingly small value, which is indicative of an insulator. In Fig. 1, the color scale corresponds to the logarithm of χ_c, clearly demonstrating a sharp transition from a metallic to an insulating phase around $U/t \approx 0.75$ at low temperatures and a smoother crossover at higher temperatures. The black dashed line denotes the contour $\chi_c = 0.01$. The fact that the compressibility jumps sharply at low temperatures but decreases smoothly at higher temperatures supports the presence of a first-order transition between the SC phase and the AFM insulating phase, ending in a critical endpoint followed by a Widom crossover line, as is expected for a Mott transition at finite temperatures [44]. The precise location of the endpoint cannot be pinpointed with our available resolution.

Electronic and magnetic spectra.—To further probe the impact of the metal-to-insulator crossover in the phase diagram of Fig. 1, we extracted the electronic Green's function $\mathcal{G}$ at long imaginary time τ, $\mathcal{G}_\mathbf{k}(\tau = \beta/2)$. Here, $\beta \equiv 1/T$ is the inverse temperature. At zero temperature and on the Fermi surface, the quantity $\tilde{Z}_\mathbf{k} = 2\mathcal{G}_\mathbf{k}(\tau = \beta/2)$

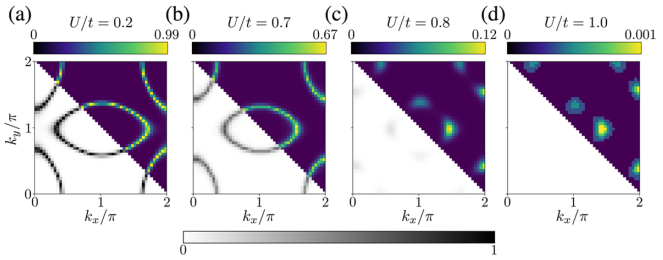

FIG. 3. Evolution of the quasiparticle spectral weight proxy, $\tilde{Z}_{\mathbf{k}}$, with interaction strength. In the upper right half (lower left half) of the panels, we plot $\tilde{Z}_{\mathbf{k}}$ for $T/t = 0.05$ in a color scale (gray scale) from 0 to $\tilde{Z}_{\max}$ (0 to 1). Note that the two halves are identical; we use two different color schemes only to highlight the loss of spectral weight across the magnetic transition. Here (a) and (b) correspond to the region prior to the AFM transition, while (c) and (d) are after. For small values of the interaction, the quasiparticle spectral weight matches the noninteracting Fermi surface shown in Fig. 1. For larger values, the Fermi surface shrinks and, beyond $U/t = 0.75$, is reconstructed, signaling the onset of AFM order with wave vector $\mathbf{Q} = (\pi, \pi)$. To produce these figures, we combined simulations from 16 different twisted boundary conditions.

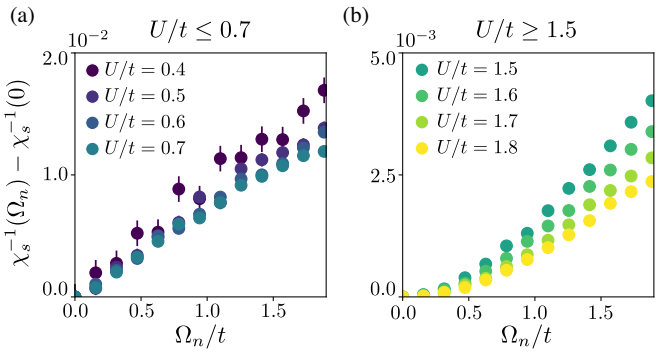

FIG. 4. Inverse dynamical spin susceptibility $\chi_s^{-1}(\Omega_n)$ in the metallic and insulating paramagnetic regions. (a) In the regime $U/t \leq 0.7$ (i.e., to the left of the AFM dome), where the system is metallic, the dependence on Ω_n is roughly linear, $\chi^{-1}(\Omega_n) \propto \Omega_n$, indicating that the magnetic fluctuations are overdamped. (b) In the regime $U/t \geq 1.5$ (i.e., to the right of the AFM dome), where the system is insulating, the magnetic fluctuations propagate ballistically, $\chi^{-1}(\Omega_n) \propto \Omega_n^2$.

is a proxy for the quasiparticle spectral weight [26,45], being equal to 1 for a noninteracting system and 0 for an insulator. Figure 3 presents $\tilde{Z}_k$ for representative values of the interaction U and for a low temperature $T/t = 0.05$. In each panel, the upper right half shows the relative spectral weight and the color scale extends to $\tilde{Z}_{\max}$, whereas the lower left half shows the absolute spectral weight and the color scale extends to 1.

Focusing first on the upper half of the panels, we note two effects upon increasing U. At $U/t = 0.7$, we see a shrinking of the Fermi surface areas, reminiscent of the so-called $s^{\pm}$-Pomeranchuk effect in multiband systems approaching an AFM instability [46,47]. At $U/t = 0.8$ and $U/t = 1.0$, we observe a Fermi surface reconstruction typical of long-range AFM order, as resulting from the folding of the Brillouin zone by the AFM wave vector (π, π). Focusing now on the lower half of the panels, we see a strong reduction of the intensity of $\tilde{Z}_k$ as U increases, signaling a sharp suppression of the quasiparticle spectral weight. In particular, for $U/t = 1.0$, the spectral weight has decreased to the point of almost vanishing, such that, for higher values of U/t, a Fermi surface can be barely defined. This loss of quasiparticle coherence is consistent with the suppression in the charge compressibility seen in Fig. 2(c).

The reduction of the quasiparticle spectral weight has a drastic effect on the magnetic fluctuation spectrum in the paramagnetic state. Prior to the onset of AFM order, the electrons are reasonably coherent, as shown in Fig. 3(a), (b). The corresponding dynamic magnetic susceptibility at the AFM wave vector $\chi_s^{-1}(\Omega_n)$, is shown in Fig. 4(a) as a function of the Matsubara frequency $\Omega_n = 2n\pi T$. In this regime, corresponding to the left of the AFM dome, the spin dynamics is overdamped, as indicated by the linear dependence $\chi_s^{-1}(\Omega_n) \sim |\Omega_n|$. This is the expected behavior arising from the decay of AFM fluctuations into collective particle-hole excitations near the Fermi surface, called Landau damping. Note that we do not expect signatures of the superconducting gap to appear here, as even the first nonzero Matsubara frequency is comparable to T_c. On the other hand, for $U/t \geq 1.5$, to the right of the AFM dome, the quadratic behavior $\chi_s^{-1}(\Omega_n) \sim \Omega_n^2$ shown in Fig. 4(b) is typical of ballistic spin dynamics, with AFM fluctuations propagating without damping. The fact that the quasiparticle spectral weight is strongly reduced for $U/t > 0.75$ suggests that this absence of damping is a consequence of the suppression of the decay channel of an AFM excitation into quasiparticles.

Discussion.—Having completely characterized the phase diagram of the electronic two-band model shown in Fig. 1, we now discuss its implications for our understanding of the intertwining between AFM and SC in the intermediate coupling regime. The appearance of an AFM dome can be rationalized by interpolating the expected behaviors in the metallic and insulating sides of the phase diagram. From a weak-coupling perspective, because the electronlike and holelike bands are not nested, the interaction strength must overcome a threshold value for AFM order to onset. From a strong-coupling perspective, the two-band model maps onto an Ising model with a strong transverse field (see Supplemental Material [34]), and as a result the ground state is a featureless, insulating quantum paramagnet. What is surprising, however, is the fact that the threshold value for U/t at the lowest temperature probed coincides (within our resolution) with the value that triggers a metal-to-insulator transition, characterized by vanishing compressibility and quasiparticle spectral weight. Additionally, we note that the onset of AFM order is not due to Fermi surface nesting, as numerical simulations of two electronlike band dispersions (not shown) also reveal a magnetic dome at similar values of U/t.

The numerical results suggest the presence of two putative AFM quantum phase transitions near $U/t \approx 0.75$ and $U/t \approx 1.5$. Of course, the AFM transition temperature could remain nonzero beyond this range, since the lowest temperature that we probe is $T/t = 0.025$. Although this makes it difficult to locate a possible quantum critical point, the fact that the AFM susceptibility is strongly suppressed for these two values of the interaction strength [as shown in Fig. 2(a)] allows us to make a meaningful comparison between them. The main difference is that long-range superconductivity appears near $U/t = 0.75$, while not even weak SC fluctuations are observed near $U/t = 1.5$. Thus, while this result supports the point of view that AFM fluctuations play an important role in promoting high-temperature superconductivity—the highest T_c in our system is a few percent of t—it also makes it clear that proximity to an AFM transition is by no means enough for superconductivity to be triggered. On the contrary, our analysis of the spin dynamics in Fig. 4 reveals that overdamped (i.e., "slow") fluctuations are much better at promoting Cooper pairing than ballistic (i.e., "fast") fluctuations. This change in the character of the spin dynamics, in turn, can be attributed to the strong suppression of the quasiparticle spectral weight shown in Fig. 3, which effectively eliminates Landau damping. It is important to note that, despite the quasiparticle spectral weight being heavily suppressed, as long as it remains finite at nonzero temperatures, superconductivity could in principle still arise [48].

Conclusion.—In conclusion, we demonstrated that a suitable two-band version of the Hubbard model can be efficiently simulated via QMC without the fermionic sign problem. The resulting phase diagram showcases various ordered states typically found in quantum materials, such as AFM, SC, and a correlated insulating phase. More importantly, our results offer an unbiased view of the rich interplay between these different degrees of freedom, demonstrating that both AFM and SC are enhanced near the metal-to-insulator transition in the intermediate-coupling regime. Future investigations of this type of model would be desirable to shed light on the fermionic properties near the onset of the AFM order, particularly to elucidate whether non-Fermi liquid behavior or pseudogap behavior is also triggered by interband repulsive interactions.

We thank A. Chubukov, A. Klein, Z. Y. Meng, and O. Vafek for fruitful discussions. M. H. C. and R. M. F. are supported by the U.S. Department of Energy, Office of Science, Basic Energy Sciences, Materials Science and Engineering Division, under Award No. DE-SC0020045. R. M. F. also acknowledges partial support from the Research Corporation for Science Advancement via the Cottrell Scholar Award. X. W. acknowledges financial support from National MagLab, which is funded by the National Science Foundation (DMR-1644779) and the state of Florida. Y. S. was supported by the Department of Energy, Office of Basic Energy Sciences, under Contract No. DE-AC02-76SF00515 at Stanford, by the Gordon and Betty Moore Foundation's EPiQS Initiative through Grant Nos. GBMF4302 and GBMF8686, and by the Zuckerman STEM Leadership Program. E. B. was supported by the European Research Council (ERC) under grant HQMAT (Grant No. 817799), the US-Israel Binational Science Foundation (BSF), the Minerva Foundation, and a research grant from Irving and Cherna Moskowitz. We thank the Minnesota Supercomputing Institute (MSI) at the University of Minnesota, where a part of the numerical computations was performed.

*Corresponding author.
rfernand@umn.edu
†Also at Stanford Institute for Materials and Energy Sciences, SLAC National Accelerator Laboratory and Stanford University, Menlo Park, California 94025, USA.
‡M. H. C. and X. W. contributed equally to this work.

[1] B. Keimer, S. A. Kivelson, M. R. Norman, S. Uchida, and J. Zaanen, From quantum matter to high-temperature superconductivity in copper oxides, Nature (London) **518**, 179 (2015).
[2] Z. P. Yin, K. Haule, and G Kotliar, Kinetic frustration and the nature of the magnetic and paramagnetic states in iron pnictides and iron chalcogenides, Nat. Mater. **10**, 932 (2011).
[3] P. Dai, J. Hu, and E. Dagotto, Magnetism and its microscopic origin in iron-based high-temperature superconductors, Nat. Phys. **8**, 709 (2012).
[4] A. Georges, L. de' Medici, and J. Mravlje, Strong correlations from hund's coupling, Annu. Rev. Condens. Matter Phys. **4**, 137 (2013).
[5] K. Haule and G. Kotliar, Strongly correlated superconductivity: A plaquette dynamical mean-field theory study, Phys. Rev. B **76**, 104509 (2007).
[6] H. Park, K. Haule, and G. Kotliar, Cluster Dynamical Mean Field Theory of the Mott Transition, Phys. Rev. Lett. **101**, 186403 (2008).
[7] E. Gull, P. Werner, X. Wang, M. Troyer, and A. J. Millis, Local order and the gapped phase of the Hubbard model: A plaquette dynamical mean-field investigation, Europhys. Lett. **84**, 37009 (2008).
[8] C. Weber, K. Haule, and G. Kotliar, Strength of correlations in electron- and hole-doped cuprates, Nat. Phys. **6**, 574 (2010).
[9] S. R. White, Density Matrix Formulation for Quantum Renormalization Groups, Phys. Rev. Lett. **69**, 2863 (1992).
[10] R. M. Noack, S. R. White, and D. J. Scalapino, Correlations in a Two-Chain Hubbard Model, Phys. Rev. Lett. **73**, 882 (1994).
[11] H.-C. Jiang and T. P. Devereaux, Superconductivity in the doped hubbard model and its interplay with next-nearest hopping t', Science **365**, 1424 (2019).
[12] R. Blankenbecler, D. J. Scalapino, and R. L. Sugar, Monte carlo calculations of coupled boson-fermion systems. I, Phys. Rev. D **24**, 2278 (1981).
[13] T. A. Maier, M. Jarrell, T. C. Schulthess, P. R. C. Kent, and J. B. White, Systematic Study of *d*-Wave Superconductivity

in the 2d Repulsive Hubbard Model, Phys. Rev. Lett. **95**, 237001 (2005).
[14] T. A. Maier, M. Jarrell, and D. J. Scalapino, Pairing interaction in the two-dimensional Hubbard model studied with a dynamic cluster quantum monte carlo approximation, Phys. Rev. B **74**, 094513 (2006).
[15] C. N. Varney, C.-R. Lee, Z. J. Bai, S. Chiesa, M. Jarrell, and R. T. Scalettar, Quantum monte carlo study of the two-dimensional fermion hubbard model, Phys. Rev. B **80**, 075116 (2009).
[16] J. P. F. LeBlanc *et al.*, Solutions of the Two-Dimensional Hubbard Model: Benchmarks and Results from a Wide Range of Numerical Algorithms, Phys. Rev. X **5**, 041041 (2015).
[17] T. Ayral and O. Parcollet, Mott physics and spin fluctuations: A unified framework, Phys. Rev. B **92**, 115109 (2015).
[18] B.-X. Zheng, C.-M. Chung, P. Corboz, G. Ehlers, M.P. Qi, R. M. Noack, H. Shi, S. R. White, S. Zhang, and G. K.-L. Chan, Stripe order in the underdoped region of the two-dimensional Hubbard model, Science **358**, 1155 (2017).
[19] E. W. Huang, C. B. Mendl, S. Liu, S. Johnston, H.-C. Jiang, B. Moritz, and T. P. Devereaux, Numerical evidence of fluctuating stripes in the normal state of high-tc cuprate superconductors, Science **358**, 1161 (2017).
[20] E. Y. Loh, J. E. Gubernatis, R. T. Scalettar, S. R. White, D. J. Scalapino, and R. L. Sugar, Sign problem in the numerical simulation of many-electron systems, Phys. Rev. B **41**, 9301 (1990).
[21] C. Wu and S.-C. Zhang, Sufficient condition for absence of the sign problem in the fermionic quantum monte carlo algorithm, Phys. Rev. B **71**, 155115 (2005).
[22] A. Abanov, A. V. Chubukov, and J. Schmalian, Quantum-critical theory of the spin-fermion model and its application to cuprates: Normal state analysis, Adv. Phys. **52**, 119 (2003).
[23] E. Berg, M. A. Metlitski, and S. Sachdev, Sign-problem–free quantum monte carlo of the onset of antiferromagnetism in metals, Science **338**, 1606 (2012).
[24] Y. Schattner, S. Lederer, S. A. Kivelson, and E. Berg, Ising Nematic Quantum Critical Point in a Metal: A Monte Carlo Study, Phys. Rev. X **6**, 031028 (2016).
[25] X. Y. Xu, K. Sun, Y. Schattner, E. Berg, and Z. Y. Meng, Non-Fermi Liquid at $(2+1)$D Ferromagnetic Quantum Critical Point, Phys. Rev. X **7**, 031058 (2017).
[26] M. H. Gerlach, Y. Schattner, E. Berg, and S. Trebst, Quantum critical properties of a metallic spin-density-wave transition, Phys. Rev. B **95**, 035124 (2017).
[27] X. Wang, Y. Schattner, E. Berg, and R. M. Fernandes, Superconductivity mediated by quantum critical antiferromagnetic fluctuations: The rise and fall of hot spots, Phys. Rev. B **95**, 174520 (2017).
[28] S. Lederer, Y. Schattner, E. Berg, and S. A. Kivelson, Superconductivity and non-fermi liquid behavior near a nematic quantum critical point, Proc. Natl. Acad. Sci. U.S.A. **114**, 4905 (2017).
[29] E. Berg, S. Lederer, Y. Schattner, and S. Trebst, Monte carlo studies of quantum critical metals, Annu. Rev. Condens. Matter Phys. **10**, 63 (2019).
[30] Z.-X. Li and H. Yao, Sign-problem-free fermionic quantum monte carlo: Developments and applications, Annu. Rev. Condens. Matter Phys. **10**, 337 (2019).
[31] Y. Motome and M. Imada, A quantum monte carlo method and its applications to multi-orbital Hubbard models, J. Phys. Soc. Jpn. **66**, 1872 (1997).
[32] J. Wu, P. Phillips, and A. H. Castro Neto, Theory of the Magnetic Moment in Iron Pnictides, Phys. Rev. Lett. **101**, 126401 (2008).
[33] A. V. Chubukov, D. V. Efremov, and I. Eremin, Magnetism, superconductivity, and pairing symmetry in iron-based superconductors, Phys. Rev. B **78**, 134512 (2008).
[34] See Supplemental Material at http://link.aps.org/supplemental/10.1103/PhysRevLett.125.247001 for further details on the numerical analysis and Refs. [35–42].
[35] F. F. Assaad, *Quantum Monte Carlo Methods on Lattices: The Determinantal Method*, Publication Series of the John von Neumann Institute for Computing (NIC) (2002).
[36] J. Gubernatis, N. Kawashima, and P. Werner, *Quantum Monte Carlo Methods* (Cambridge University Press, Cambridge, England, 2016).
[37] M. E. Fisher and M. N. Barber, Scaling Theory for Finite-Size Effects in the Critical Region, Phys. Rev. Lett. **28**, 1516 (1972).
[38] K. Binder and D. P. Landau, Finite-size scaling at first-order phase transitions, Phys. Rev. B **30**, 1477 (1984).
[39] A. M. Ferrenberg and R. H. Swendsen, New Monte Carlo Technique for Studying Phase Transitions, Phys. Rev. Lett. **61**, 2635 (1988).
[40] D. J. Scalapino, S. R. White, and S. Zhang, Insulator, metal, or superconductor: The criteria, Phys. Rev. B **47**, 7995 (1993).
[41] A. W. Sandvik, Computational studies of quantum spin systems, AIP Conf. Proc. **1297**, 135 (2010).
[42] M. S. L. du Croo de Jongh and J. M. J. van Leeuwen, Critical behavior of the two-dimensional Ising model in a transverse field: A density-matrix renormalization calculation, Phys. Rev. B **57**, 8494 (1998).
[43] F. P. Toldin, M. Hohenadler, F. F. Assaad, and I. F. Herbut, Fermionic quantum criticality in honeycomb and π-flux Hubbard models: Finite-size scaling of renormalization-group-invariant observables from quantum monte carlo, Phys. Rev. B **91**, 165108 (2015).
[44] H. Terletska, J. Vučičević, D. Tanasković, and V. Dobrosavljević, Quantum Critical Transport Near the Mott Transition, Phys. Rev. Lett. **107**, 026401 (2011).
[45] N. Trivedi and M. Randeria, Deviations from Fermi-Liquid Behavior above T_c in 2d Short Coherence Length Superconductors, Phys. Rev. Lett. **75**, 312 (1995).
[46] L. Ortenzi, E. Cappelluti, L. Benfatto, and L. Pietronero, Fermi-Surface Shrinking and Interband Coupling in Iron-Based Pnictides, Phys. Rev. Lett. **103**, 046404 (2009).
[47] A. V. Chubukov, M. Khodas, and R. M. Fernandes, Magnetism, Superconductivity, and Spontaneous Orbital Order in Iron-Based Superconductors: Which Comes First and Why?, Phys. Rev. X **6**, 041045 (2016).
[48] Y. Wang, A. Abanov, B. L. Altshuler, E. A. Yuzbashyan, and A. V. Chubukov, Superconductivity Near a Quantum-Critical Point: The Special Role of the First Matsubara Frequency, Phys. Rev. Lett. **117**, 157001(2016).